

# Ligand-dependent exciton dynamics and photovoltaic properties in PbS quantum dot heterojunction solar cells

Cite this: DOI: 10.1039/x0xx00000x

Received 00th January 2012,  
Accepted 00th January 2012

DOI: 10.1039/x0xx00000x

www.rsc.org/

Jin Chang,<sup>a,b</sup> Yuhei Ogomi,<sup>c,e</sup> Chao Ding,<sup>b</sup> Yao Hong Zhang,<sup>b</sup> Taro Toyoda,<sup>b,e</sup>  
Shuzi Hayase,<sup>c,e</sup> Kenji Katayama,<sup>d</sup> and Qing Shen<sup>\*b,e</sup>

The surface chemistry of colloidal quantum dots (QDs) plays an important role in determining the photoelectric properties of QD films and the corresponding quantum dot heterojunction solar cells (QDHSCs). To investigate the effects of ligand structure on the photovoltaic performance and exciton dynamics in QDHSCs, PbS QDHSCs were fabricated by the solid state ligand exchange method with mercaptoalkanoic acid as the cross-linking ligands. Temperature-dependent photoluminescence and ultrafast transient absorption spectra show that the electronic coupling and charge transfer rate within QD ensembles were monotonically enhanced as the ligand length decreasing. However, in practical QDHSCs, the second shortest ligand 3-mercaptopropionic acid (MPA) gave a higher power conversion efficiency than that of the shortest thioglycolic acid (TGA) ligand. This could be attributed to their difference in surface trap state, supported by thermally stimulated current measurements. Moreover, compared with the non-conjugated MPA, the conjugated ligand 4-mercaptopbenzoic acid (MBA) introduces less trap states and similar charge transfer rate in QD ensembles, but results into poor photovoltaic properties. This unexpected result could be contributed to the QD-ligand orbital mixing, leading to the charge transfer from QDs to ligands instead of charge transfer between adjacent QDs. This work highlights the significant effects of ligand structures on the photovoltaic properties and exciton dynamics in QDHSCs, which would shed light on the further development of QD-based photoelectric devices.

## Introduction

Solar cells based on colloidal quantum dots (QDs) have been one of the most promising candidates for the third-generation photovoltaics due to their optimal match with the sun's spectrum, high molar extinction coefficient, multi-exciton generation (MEG) possibility, and the advantage of low-cost manufacture through solution-processing techniques.<sup>1-3</sup> In the past few years, quantum dot solar cells (QDSCs) have developed rapidly and attracted increasing attention. The power conversion efficiency (PCE) records of both sensitized and heterojunction QDSCs have achieved over 10%,<sup>4, 5</sup> which indicates their great potential for commercialization. In comparison with high performance sensitized cells (mostly liquid state), quantum dot heterojunction solar cells (QDHSCs) obviously have an extra advantage in the device stability due to their all-solid-state configuration. On the other hand, QDHSCs require finer control over the surface chemistry and self-assembly of QDs because photo-generated charges have to diffuse through numerous interfacial barriers in QD solids before they are collected by charge transport materials or metal contacts.

The photovoltaic performance of QDHSCs is significantly dependent on the surface passivation or modification of QDs. In

general, two main strategies are often applied for this purpose: i) formation of core/shell structure by coating QD surfaces with wide band-gap semiconductors or insulating materials;<sup>6</sup> ii) surface passivation with atomic or molecular ligands through ligand exchange methods.<sup>7-9</sup> For the first approach, the surface trap states of QD cores can be well-passivated by the shell materials, thus reduce the charge recombination at QD surfaces. However, inorganic shells tend to hinder the effective charge transfer between neighbouring QDs, which would significantly deteriorate the current generation in QDHSCs. In contrast, the second approach also provides effective surface passivation for QDs, while does not have to sacrifice the photocurrent due to the tailored ligand structure. Up to date, high performance QDHSCs are mostly fabricated by using atomic ligands, but molecular ligands still attract much attention because they offer wide opportunities to obtain interesting phenomena and they are ideal models to investigate the QD coupling and exciton behaviour in QDHSCs.

In the past few years, many techniques have been applied to examine the photoelectric properties of QDs or QD-organic systems. For example, transient photoluminescence (tPL) measurements revealed that the charge transfer rate and/or non-

radiative energy transfer (NRET) rate of PbS QD assemblies was linearly increased as narrowing the QD-QD spacing by tailoring the ligand length.<sup>10-12</sup> Similar trend of ligand-length dependent photoelectric properties were determined from steady state PL quenching and field-effect transistor (FET) measurements.<sup>13, 14</sup> Although ultrafast transient absorption (TA) spectroscopy has been applied to examine the exciton relaxation processes in various systems,<sup>15-18</sup> it has rarely been employed to investigate the exciton relaxation dynamics in assembled QD arrays. In addition, previous studies mostly ignore or did not pay much attention to the trap states, which is highly related with other radiative and non-radiative behaviour of excitons. Moreover, although short ligands such as 3-mercaptopropionic acid has been demonstrated as an effective ligand in QDHSCs, there is a lack of systematic investigation on the relationship between ligand structure and photovoltaic performance of QDHSCs. Our work was motivated by the assumption that the photovoltaic performances of QDHSCs probably could be enhanced by extremely narrowing the QD distance through proper ligands. This work was also motivated by the curiosity that whether conjugated ligand would serve as conduits between QDs and thus enhance the photoelectric properties. Alivisatos *et al.* reported that an abnormally high mobility was observed in QD films with tetrathiafulvalene-tetracarboxylate as the surface ligand, which was attributed to the reduced QD-QD barrier height caused by the near-resonant alignment of the QD  $1S_h$  state and molecular orbital state.<sup>19</sup> Similarly, Giansante *et al.* demonstrated that the optical absorption intensities of colloidal PbS QDs with conjugated ligands are much higher compared to that of non-conjugated ligand. The corresponding reason was proposed to be due to the ground-state ligands/QD orbital mixing, and the enhanced electronically coupling between ligands and QDs.<sup>20</sup> These results reflect the superiority of conjugated ligands in light harvest and carrier transport in QD colloidal and films, but detailed comparison between conjugated and non-conjugated ligands was not examined for practical QDHSCs.

In this work, we systematically investigate the effects of ligands on the photoelectric properties of QD solids and the corresponding solar cells. PbS QD films were fabricated by the layer-by-layer method using mercaptoalkanoic acids (MAA) for solid-state ligand exchange. The influences of alkyl chain length and molecular conjugation on the photovoltaic performance and exciton/charge dynamics in PbS QDHSCs were investigated. Experimental results verified that the exciton dissociation rate increased significantly with decreasing the ligand length, but the highest efficient device was obtained by using the second shortest ligand. Although the shortest ligand favoured the exciton dissociation or charge transfer between adjacent QDs, it was supposed to introduce more trap states, which might be deleterious for the carrier transport and charge collection. In the case of conjugated ligand, device performances were also unexpectedly due to the specific QD-ligand interaction.

## Experimental

### Materials

Lead oxide (PbO, 99.5%), oleic acid (OA, technical grade, 60%), cadmium chloride ( $CdCl_2$ , 95.0%), hexadecyltrimethyl ammonium bromide (CTAB, 99.0%), oleylamine (OLA, 99.0%), thioglycolic acid (TGA, 95.0%) and oxalic acid (OXA, 99.0%) were purchased from Wako Pure Chemical Industries. 1-octadecene (ODE, 95.0%), tetradecylphosphonic acid (TDPA, 97%), 3-mercaptopropionic acid (MPA, 99.0%), 6-

mercaptohexanoic acid (MHA, 90%), 16-mercaptohexadecanoic acid (MHDA, 90.0%), 4-mercaptopbenzoic acid (MBA, 99%) and hexamethyldisilathiane (TMS, synthesis grade) were purchased from Sigma-Aldrich. All chemicals were used as received without purification.

### Synthesis of QDs

The synthesis of colloidal PbS QDs is similar to our previously reported method.<sup>21</sup> A mixture of PbO (1.34 g, 6 mmol), oleic acid (4.23 g, 15 mmol) and ODE (50 mL) was degassed at 80 °C for 1 h. The obtained solution was heated to 115 °C and kept at this temperature for 2 h under  $N_2$ , followed by the injection of TMS solution (a mixture of 630  $\mu$ L, 3 mmol TMS and 10 mL pre-degassed ODE). After injection, the obtained colloidal was allowed to cool down to 70 °C, followed by the injection of a halide precursor (a mixture of 1 mmol  $CdCl_2$ , 0.1 mmol TDPA and 3 g OLA). After cooling down to room temperature, QDs were isolated by adding acetone and centrifugation. The supernatant was discarded and the precipitate was purified by successive dispersion in toluene and precipitation with a mixture of acetone and methanol, and finally dispersed in octane with concentration of 50 mg  $mL^{-1}$ .

### Fabrication of solar cells

As-prepared PbS colloidal QDs were applied for the fabrication of QDHSCs using ZnO-nanowires (ZnO-NWs) as the electron transporting layer with the NW thickness around 1  $\mu$ m. Briefly, PbS QD layers were deposited on ZnO-NWs using a layer-by-layer method. For each layer, 110  $\mu$ L of QD colloidal was spin-cast onto ZnO-NWs substrate at 2500 rpm for 15 s. Then, a ligand solution in methanol (10 mM) was dropped on the substrate and spun dry after a 5 s wait. The substrate was finally rinsed three times with methanol, followed by baking at 100 °C for 30 s. This process was repeated 25 cycles to fill in ZnO-NW arrays and achieve ~300 nm QD overlayer above ZnO. The QD deposition procedures were performed under ambient conditions. Au electrode with thickness around 100 nm was thermally evaporated on QD layers through a shadow mask under a pressure of  $10^{-5}$  mbar.

### Characterization of QDs and solar cells

The surface chemistry of ligand-capped QD films was characterized by fourier transform infrared (FT-IR) spectra using a Nicolet 6700 FT-IR spectrometer with the reflective mode. The microstructure of QD ensembles was examined by a high resolution transmission electron microscopy (HR-TEM, JEOL, JEM-2100F). To prepare samples for HR-TEM characterization, as-prepared QD colloidal (10 mg  $mL^{-1}$  in hexane) was dropped on an ultrathin carbon film and naturally dried in air. Then, the film was dipped alternately into a ligand solution (10 mM in methanol) for 5 s and a rinsing solution of methanol for 30 s, followed by drying in air. UV-vis-NIR absorption spectra of QD colloidal and films were measured using a JASCO V-670 spectrophotometer. Temperature dependent PL spectra were measured using a LabRAM HR-800 spectrometer (Horiba Jobin Yvon, France) with the temperature ranging from 77 K to 298 K. Transient absorption (TA) spectra were measured using a titanium/sapphire laser (CPA-2010, Clark-MXR, Inc.) with a repetition rate of 1 kHz and a pulse width of 150 fs. The wavelengths of the pump and probe light are 650 nm and 1100 nm, respectively.

Thermally stimulated current (TSC) measurements were conducted by a thermally stimulated femtoampere electron trap tracer (TS-FETT) system (Rigaku, Japan) in a similar way described in previous reports.<sup>22, 23</sup> At low temperature (95 K), traps in substrate were filled with carriers by exposing visible light of 635 nm to the sample. After light exposure, the sample was heated gradually. Those trapped electrons were released and detected as TSC as the temperature increases.

The current density-voltage ( $J$ - $V$ ) curves were recorded using a Keithley 2400 sourcemeater under simulated solar light illumination (1 sun, 100 mW cm<sup>-2</sup>) generated by a Peccell PEC-L10 solar simulator. The light intensity was calibrated with a silicon diode (BS-520BK, Bunkoukeiki) before each measurement. All measurements were performed by both forward and reverse scans (10 mV voltage steps and 200 ms delay times) under air conditions, and the average data was extracted to plot the  $J$ - $V$  curves. Incident photon-to-current efficiency (IPCE) measurements were conducted using a Nikon G250 monochromator equipped with a 300 W Xe arc lamp. Transient voltage decay curves were measured using a 532 nm pulsed laser without bias illumination. The pulse duration was 5 ns and the repetition rate was set as 4 Hz. The voltage responses were recorded using a digital oscilloscopes (DS-5554, Iwatsu).

## Results and Discussion

### Surface chemistry and microstructure of QD ensembles

Before examining the effects of surface ligands on photoelectric properties of PbS QDHSCs, the surface chemistry and microstructure of PbS QD ensembles were investigated by FT-IR and HR-TEM measurements, respectively. Fig. 1 shows the FT-IR spectra of PbS QD films with various ligands in the range of 3200-2500 cm<sup>-1</sup>. It is presented that the OA-capped PbS QD film (PbS-OA) exhibited strong peaks at 2924 and 2853 cm<sup>-1</sup>, which are assigned to the asymmetric and symmetric CH<sub>2</sub> stretches, respectively. The shoulder peak at 2955 cm<sup>-1</sup> and weak peak at 3006 cm<sup>-1</sup> are specifically assigned to the asymmetric CH<sub>3</sub> stretch and CH (-C=C-H) stretch of oleic acid. After ligand exchange with MAA ligands, both above peaks (2955 and 3006 cm<sup>-1</sup>) disappeared, indicating the removal of oleic acid. The replacement of OA ligands was also verified by the decreasing CH<sub>2</sub> stretch vibrational peak areas with decreasing the chain length of MAA ligands. Within experimental uncertainty, the integrated CH<sub>2</sub> peak area was proportional to the number of -CH<sub>2</sub>- repeating units in capping ligands. Besides, the absence of SH stretching vibrational peaks in the range of 2550-2600 cm<sup>-1</sup> suggested that sulfur atoms of thiols were bonded with unsaturated lead atoms on QD surfaces. Fig. S1 shows two sets of peaks in the range of 1551-1515 cm<sup>-1</sup> and 1463-1415 cm<sup>-1</sup>, which are attributed to the asymmetric and symmetric carboxylate stretches, respectively, indicating the chemical binding of ligands on QD surfaces. The binding structure of carboxylate molecules with metal elements have been well-established, which mainly consist of bidentate (bridging and chelating) and monodentate modes.<sup>24</sup> In the case of PbS QDs, Cass et al. assigned the bridging bidentate peak at 1553 cm<sup>-1</sup>, and chelating bidentate peak at 1525 cm<sup>-1</sup>.<sup>25</sup> In this work, the peaks around 1551 cm<sup>-1</sup>, 1531 cm<sup>-1</sup>, and 1515 cm<sup>-1</sup> could be assigned to the bridging bidentate, chelating bidentate, and monodentate modes, respectively. It was noted that PbS-OA was dominated with the chelating bidentate and monodentate modes, while MAA-capped QDs were dominated with chelating bidentate mode (with the exception of TGA), which could be due to the

steric effects of ligands. According to above discussion, QDs are considered as cross-linked by MAA ligands after ligand exchange, instead of isolated by OA ligands (Fig. 2).

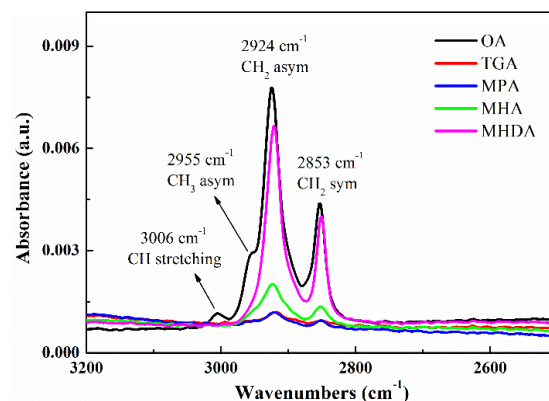


Fig. 1 Reflective FT-IR spectra (3200-2500 cm<sup>-1</sup>) of PbS QD films with various surface ligands: OA, TGA, MPA, MHA and MHDA.

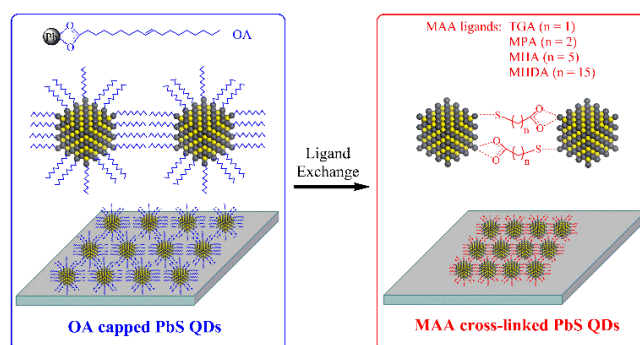


Fig. 2 Schematic comparison of PbS QD films before and after the ligand exchange with MAA ligands.

To examine the effects of ligands on the assembly of PbS QDs, single layer QDs were deposited on ultrathin carbon film and characterized by HR-TEM. Fig. 3 shows the TEM images of PbS QD ensembles with various ligands and the statistic QD-QD spacing. The inter-particle spacing was estimated through subtracting the central distance between neighbouring QDs by the QD diameter. It was observed in Fig. 3a and 3b that the average diameter of OA-capped PbS QDs was around 3.7±0.1 nm. The average QD-QD spacing of PbS-OA film was around 3 nm (inset of Fig. 3a), which is slightly less than twice the length of OA ligand, suggesting the separation of QDs by interdigital OA ligands.<sup>26</sup> By comparing all TEM images of QD films, it was clearly shown that the borderlines of PbS-MAA QDs were more distinct than that of PbS-OA, which was in good agreement with the removal of OA ligands from QD surfaces. In addition, relatively short MAA ligands (TGA, MPA) gave closely packed “quasi-2D” QD films, while long ligands (MHA, MHDA) lead to loosely assembled QD films (Fig. 3c-3j). The average QD-QD spacing was calculated as 0.8 nm, 1.0 nm, 1.5 nm and 3.0 nm for TGA, MPA, MHA and MHDA ligands, respectively. The QD-QD spacing in QD films was found to be linearly dependent on the number of carbon atoms of corresponding ligands (Fig. 4). This is consistent with the MAA-crosslinked QD model as illustrated in Fig. 2.

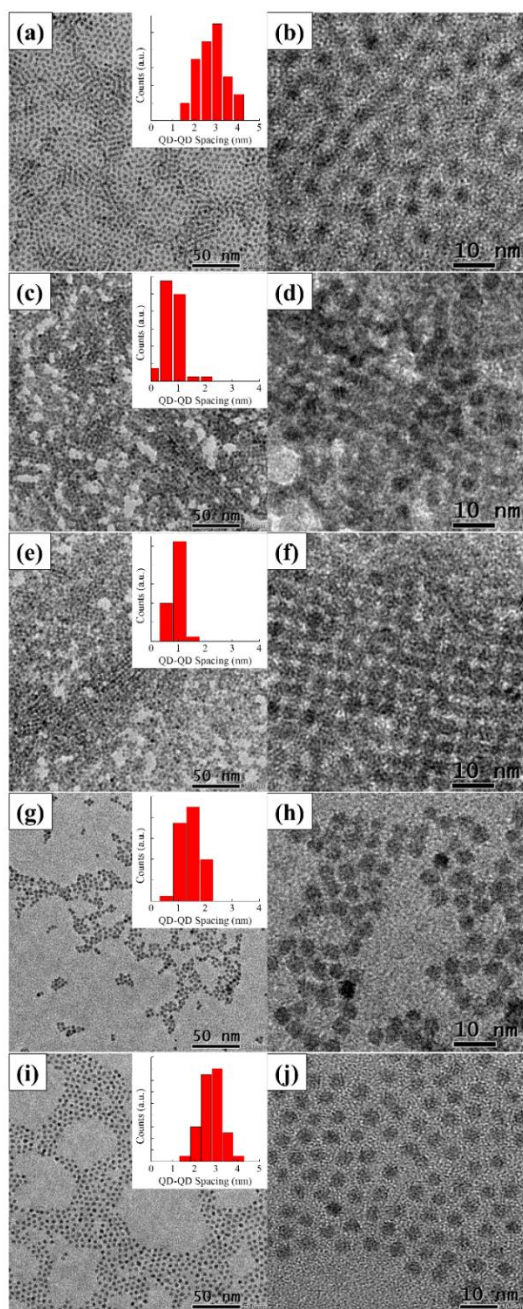


Fig. 3 TEM images of PbS QDs capped with various surface ligands: (a,b) OA; (c,d) TGA; (e,f) MPA; (g,h) MHA and (i,j) MHDA. The inset figures are the corresponding QD size distribution.

The ligand dependent self-assembly behaviour of PbS QDs was also investigated by the steady state optical absorption measurement. QD films were fabricated by spin-coating PbS colloidal on cleaned glasses for one cycle with or without the ligand exchange process. Within experimental uncertainty, the total amount of QDs was approximately same for all QD-assembled films, while the QD density is dependent on capping ligands. Fig. S2 shows the UV-vis-NIR absorption spectra of PbS QD-assembled films with various ligands. It is shown that the absorption intensity of QD films was highly related with the ligand length. The absorption intensity was much lower in the case of long ligands (MHDA and OA) than that of short ligands

(TGA, MPA and MHA). This ligand dependent absorption intensity could be attributed to the diversity of QD assemble density, as presented in Fig. 3.

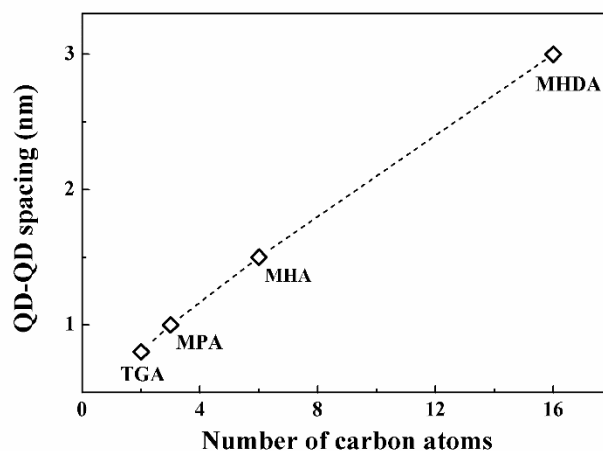


Fig. 4 The linear relationship between the QD-QD spacing and the number of carbon atoms of capping ligands.

#### Ligand length effects on photovoltaic properties and exciton/charge dynamics

In order to evaluate the ligand length effects on the photovoltaic performances and charge dynamics in quantum dot solar cells and therefore determine the optimum ligand, PbS QDHSCs were fabricated by assembling PbS QDs on ZnO nanowires (ZnO-NWs) using a layer-by-layer method. Fig. 5a and 5b show the cell structure and the representative current density-voltage ( $J$ - $V$ ) curves of PbS QDHSCs with different ligands, respectively. The extracted average photovoltaic parameters are summarized in Table S1. It was shown that the solar cells with MHDA ligand were electrically disconnected due to the large QD-QD spacing in PbS-MHDA QD film. The PCE values of PbS QDHSCs based on different ligands show the trend of MPA > TGA > MHA. The MPA-based cells exhibited the best efficiency of 2.64%, which was mainly attributed to the highest short-circuit current density ( $J_{sc}$ ). This outcome is contrary to our previous prediction that the shortest ligand TGA would give the best photovoltaic performance due to the shortest QD-QD spacing. In addition, the solar cells based on longer ligand MHA exhibited the lowest  $J_{sc}$  and PCE values, but show the highest open-circuit voltage ( $V_{oc}$ ) value of 0.53 V.

The incident photon conversion efficiency (IPCE) and the open-circuit voltage decay (OCVD) were measured to further evaluate the ligand length effects on the photovoltaic performances of PbS QDSCs. As shown in Fig. 5c, the IPCE values of PbS QDHSCs with different ligands follow the order of MPA > TGA > MHA (especially in the range of 400-600 nm), which is consistent with that of  $J_{sc}$  values. The short and long wavelength incident light can respectively reach the shallow and deep position of PbS solid from the FTO side. The IPCE result indicated that the charge injection and/or collection efficiency of MPA-based device was higher than that of TGA and MHA-based device. By comparing the IPCE spectra in the range below and above 600 nm, it could be deduced that the photocurrent was mostly determined by the hole transport property because electrons could be easily injected into ZnO-NWs (especially in the range below 600 nm). The low  $J_{sc}$  and IPCE values in MHA-

based cell was attributed to the large QD-QD spacing, which resulted in poor charge transport properties in PbS-MHA solid. On the other hand, the high  $V_{oc}$  in MHA-based QDHSCs was attributed to the reduced charge recombination, which was supported by the OCVD curves as shown in Fig. 5d.

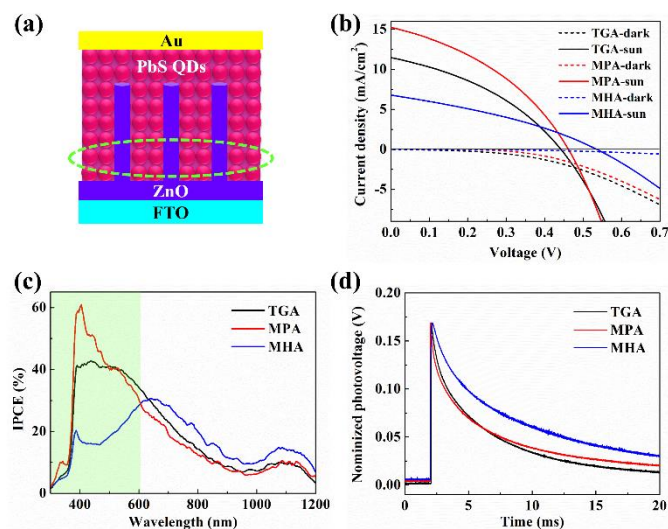


Fig. 5 (a) Illustration of the solar cell configuration based on PbS QDs and ZnO-NWs. The  $J$ - $V$  curves (b), IPCE spectra (c) and open-circuit voltage decay curves (d) of PbS QDHSCs with different ligands.

To investigate the mechanism behind above experimental results, the exciton dynamics within PbS QD ensembles were systematically characterized by PL, TA and TSC measurements. Upon illumination, photo-generated exciton relaxes through radiative recombination (PL emission) and non-radiative recombination paths. The non-radiative recombination processes in QD ensembles mainly contains: i) charge trapping through inner and/or interfacial defects, ii) exciton dissociation between adjacent QDs, iii) exciton dissociation between QDs and surface ligands, iv) energy transfer in disordered QD ensembles. In this work, the third and fourth processes for QDs with non-conjugated ligands could be eliminated for the following reasons. First, the possibility of charge transfer from QDs to ligands was impossible owing to the large energy gap and insulating nature of non-conjugated ligands. Second, the energy transfer between QDs usually occurs in the presence of QDs with various size distribution.<sup>12</sup> The QDs used in this study had a very narrow size distribution of  $\pm 3\%$  and all QD ensembles were fabricated with the same batch of colloidal QDs, suggesting the QD-QD energy transfer process could be negligible. Therefore, for the sake of simplicity, the exciton relaxation processes in QD ensembles are supposed to mainly includes charge trapping, charge transfer between adjacent QDs, and radiative emission (Fig. 6).

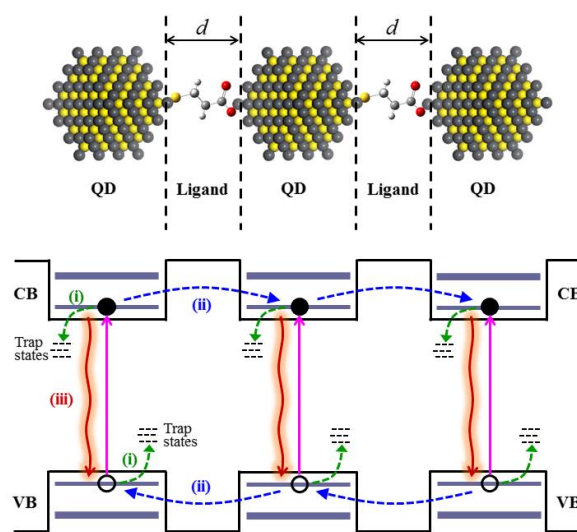


Fig. 6 Illustration of the exciton relaxation processes in MAA ligand-linked QD ensembles, which mainly includes: i) charge trapping, ii) exciton dissociation (i.e. charge transfer) between adjacent QDs, and iii) radiative PL emission. The solid and hollow dots represent photo-generated electrons and holes, respectively.

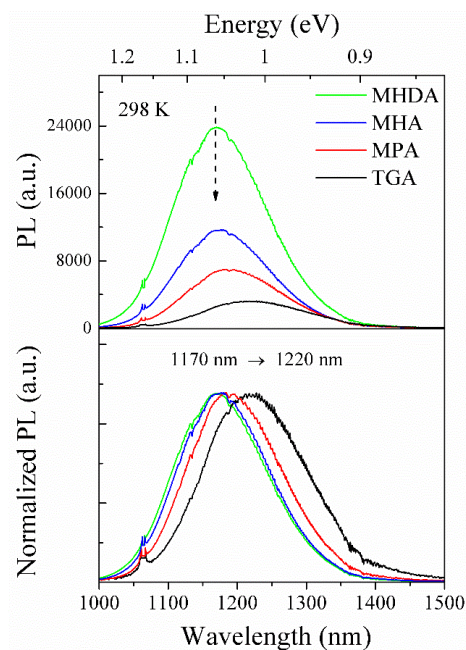


Fig. 7 Room temperature PL emission and the normalized spectra of PbS QD films with different MAA ligands.

Temperature dependent PL spectra of PbS QD films were measured at various temperature with the excitation wavelength of 514 nm. Fig. 7 shows the room temperature PL spectra and the normalized spectra of PbS QD films with different length MAA ligands. It was observed that the PL intensity monotonically decreased as decreasing the ligand length. This suggests that the non-radiative recombination, i.e. charge trapping and/or charge transfer are enhanced by shorter ligands. It was also shown in Fig. 7 that the PL peak was red-shifted from

1170 nm to 1220 nm when the ligand length decreases. The red-shift of PL peaks was attributed to the enhanced electronic coupling between closely-packed QDs. The low temperature (77 K) PL spectra (Fig. S3) have the same trend with the room temperature result. Fig. S4 shows the PL spectra versus temperature (77-298 K) for QD films with different length MAA ligands. It was found that PL peaks were blue-shifts as increasing temperature, and shorter ligands correspond to larger shifts. The integrated PL intensity versus temperature for QD films with different length ligands was plotted and presented in Fig. 8. As temperature increasing, the integrated intensity decreases monotonically for QD films with TGA and MHA ligands. However, in the case of MPA ligand, it can be seen that the integrated intensity was nearly constant as temperature increasing. It was suspected that the temperature-independent integrated PL intensity of PbS-MPA probably was associated with the unexpected photovoltaic properties in the MPA-based QDHSCs. It was commonly accepted that the PL emission tends to be quenched as the temperature increasing due to the thermally enhanced charge trapping and/or transfer. Although trapped charge at dark states was found to be able to migrate back to bright states and enhance PL intensity at low temperatures (< 100 K), the overall trend of PL intensity drops as temperature increasing.<sup>27, 28</sup> The unexpected temperature-independent integrated PL intensity of PbS-MPA was probably attributed to the few trap states, which was confirmed by the experimental results of TSC measurements as mentioned later. To deeply explore the ligand effects on the photoelectric properties of QDs, it is demanded to separately investigate the charge trapping and charge transfer dynamics in QD ensembles.

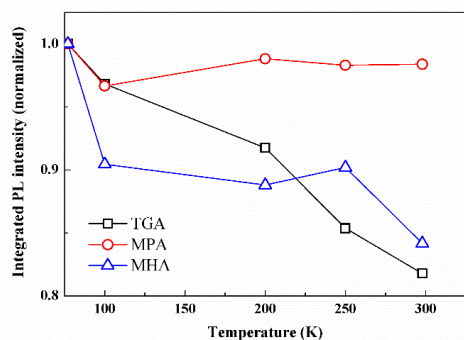


Fig. 8 Integrated PL intensity versus temperature (77-298 K) for PbS QD films with different length ligands.

For the above purpose, ultra-fast transient absorption (TA) spectra were measured for PbS QD films with MAA ligands of different length in the time scale of 1 ns. The probe beam wavelength chosen in the TA measurement was 1100 nm, which just corresponded to the optical absorption between LUMO and HOMO in the QD solids (i.e. the optical absorption of the lowest excited state). In this case, it is known that the absorbance change ( $\Delta A$ ) in TA measurements is proportional to the exciton density  $n$  at the lowest excited states in the QDs.<sup>29</sup> In consideration of the two-carrier and three-carrier recombination processes, TA decay curves can be represented by the following equation:<sup>30</sup>

$$\frac{dn}{dt} = An + Bn^2 + Cn^3 \quad (1)$$

where  $An$  represents single-carrier behaviour,  $Bn^2$  represents two-carrier radiative recombination (i.e. PL emission), and  $Cn^3$

represents three-carrier Auger recombination process. Fig. S5 shows the TA spectra of PbS-MPA QD film with different excitation fluences. The result shows multi-exponential decay curves under strong excitation fluences, corresponding to the two-carrier and/or three-carrier recombination processes. In contrast, a single exponential decay was observed under weak excitation fluence, which corresponded to the single-carrier behaviour (e.g. exciton dissociation and/or trapping). In order to specifically investigate the single-carrier behaviour in QD ensembles, a weak excitation fluence of  $27.5 \mu\text{J}/\text{cm}^2$  was applied. For the PbS-MHDA film where QD-QD spacing was relatively large, the TA signal (Fig. 9) was constant, which was identical with that of PbS-OA colloidal (Fig. S6). This indicated that charge transfer does not occur in isolated QDs and/or charge trapping does not occur within the timescale of 1 ns. For QD films with shorter ligands, the TA kinetics were fitted well with one exponential decay with lifetime  $\tau$ . As shown in Fig. 9, the exciton lifetime decreased rapidly from 68 ns to 3.4 ns as the ligand length decreasing. Interestingly, the exciton dissociate rate (the inverse value of the exciton lifetime) is found to be a single exponential decay function of the QD distance, which can be described very well by the Marcus theory.<sup>31</sup> This result strongly indicates that single-carrier behaviour of the exciton relaxation measured by the TA in the ultrafast time scale is charge transfer between the adjacent QDs rather than charge trapping. According to our results, it can be concluded that the charge transfer (i.e., exciton dissociation) in MAA-capped QD films is dominated by the tunnelling mechanism, and shorter ligands lead to faster charge transfer rate (Figure 10).

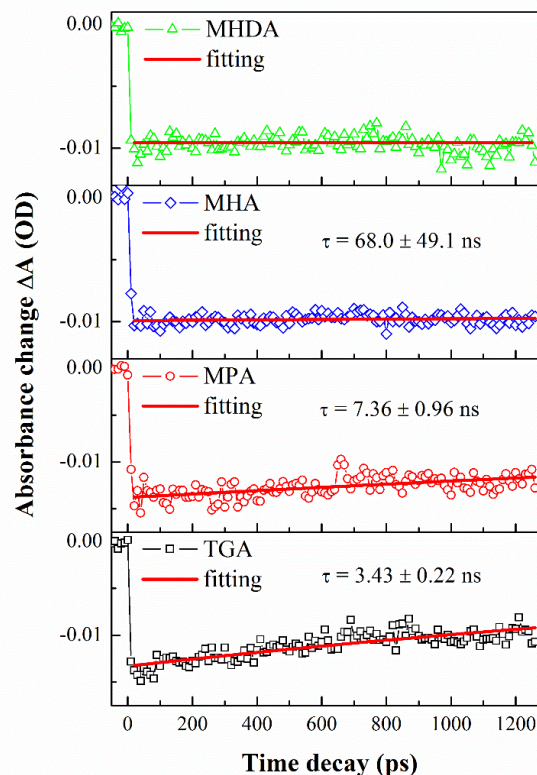


Fig. 9 Comparison of the ultra-fast TA spectra of PbS QD films with different length MAA ligands. All samples were pumped by 650 nm laser pulse with the excitation fluence of  $27.5 \mu\text{J}/\text{cm}^2$ , and probed at 1100 nm. The red solid lines are fitting curves.

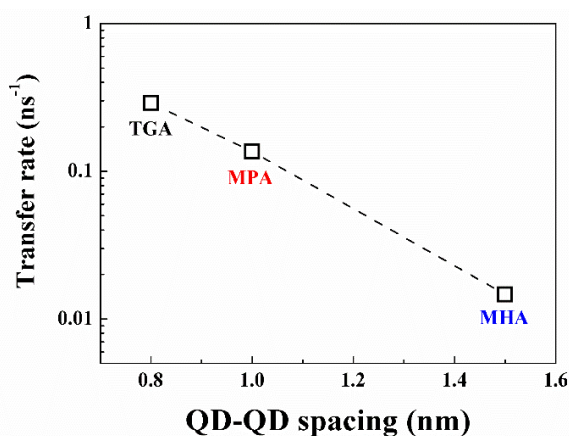


Fig. 10 Plot of the charge transfer rates (calculated from the exciton lifetimes in Fig. 9) versus QD-QD spacing measured with HR-TEM. The single exponential decay indicates that the charge transfer occurs via tunnelling mechanism according to the Marcus theory.

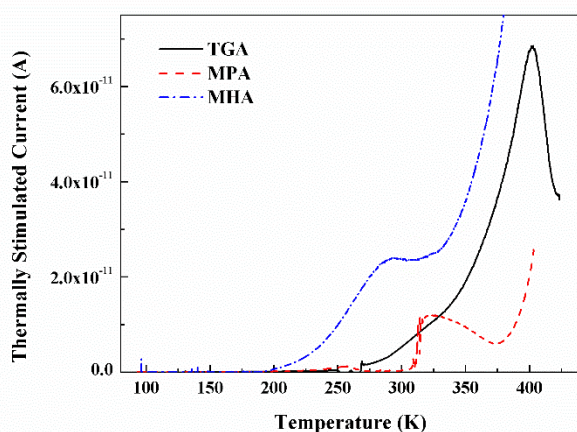


Fig. 11 TSC curves of PbS QD films capped with TGA, MPA and MHA ligands, respectively.

Apart from the TA measurements to investigate the charge transfer between adjacent QDs, TSC technique was carried out to investigate the electronic trap states in PbS QDs with different ligands. TSC is a powerful method for researchers to obtain the trap state information in semiconducting materials.<sup>23, 32-34</sup> At low temperature, defects in QD ensembles were filled with electrons under light exposure. The trapped electrons were then released by slowly heating up samples, and the stimulated current is recorded as a function of temperature (see the set up in Fig. S7). The TSC signal at a higher temperature is related to the electrons from deeper traps and the TSC signal at a lower temperature is associated with shallow traps. In other words, the TSC intensity is associated with the amount of trapped electrons, and the temperature at which TSC signal is associated with trap depth.<sup>23</sup> Fig. 11 shows the TSC curves (the relationship between current and temperature) of PbS QD films capped with TGA, MPA and MHA ligands, respectively. It can be seen that the second shortest ligand MPA gives the weakest TSC signal, indicating PbS-MPA possesses less trap states compared with TGA and MHA. Particularly, the TSC signal in PbS-MPA was negligible below 310 K, which is consistent with the temperature-

dependent PL curves (Fig. 8). The high density of rap states in PbS-TGA and PbS-MHA might decrease charge transport/collection efficiencies and therefore lead to poor photovoltaic performance. It should be noted the photovoltaic behaviour of PbS QDHSCs are more complicated than that of single-layer PbS QD ensemble. The highest trap density in PbS-MHA abnormally gave the highest  $V_{oc}$  value in QDHSC. In fact,  $V_{oc}$  is also dependent largely on the charge recombination at the interface of ZnO-NWs and PbS QDs. One possibility for the higher  $V_{oc}$  value in the case of PbS-MHA is that the recombination at ZnO/PbS interfaces was influenced by the PbS surface ligand. The interfacial recombination was probably decreased in the case of MHA compared to MPA and TGA, resulting from the longer distance between ZnO and PbS QDs due to the longer length of MHA ligand.

According to above experimental results, it can be concluded that the photovoltaic performances of PbS QDHSCs are not inversely proportional to the length of ligands (or QD-QD spacing). This is due to the fact that although charge transfer and electronic coupling are proportional to the ligand length, the surface passivation effect and trap states are independent with the ligand length. The shortest ligand TGA enables the strongest QD coupling and the fastest charge transfer, while possesses high trap state density at the same time. Longer ligand MHA significantly inhibits the charge transfer efficiency and therefore cause the poor photovoltaic performance, especially the poor short circuit current. It seems that the trap state density dominates the photovoltaic performance for ligands TGA and MPA. Therefore, the second shortest MPA which possesses less surface trap states leads to the best photovoltaic performance.

#### Ligand scaffold effects on photovoltaic performance and charge dynamics

Inspired by recent studies about ligand-assisted charge transport between QDs,<sup>19</sup> the ligand scaffold effects on photovoltaic performance and charge dynamics of QDHSCs were investigated in this work. It is known that conjugated molecules usually have higher conductivity than non-conjugated ones. Therefore, conjugated molecule MBA was chosen as the capping ligands for PbS QDHSCs. It has similar molecular length with MPA, but contains benzene units rather than saturated chains. Fig. S8 shows the TEM image and the statistic QD-QD spacing of PbS QDs linked with MBA ligands. The average interparticle spacing was around 1.5 nm for PbS-MBA QDs, which was more similar to that of the PbS-MHA QDs than that of PbS-MPA QDs. Fig. S9 displays the comparison of optical absorption spectra of QD films with different ligands. It was shown that the absorption of PbS-MBA QDs was obviously stronger than that of MPA, which was probably due to the ground-state ligand/QD orbital mixing.<sup>20</sup>

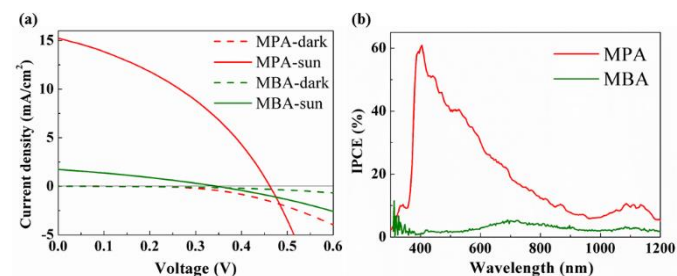


Fig. 12 Comparison of the  $J$ - $V$  curves (a) and IPCE spectra (b) of QDHSCs based on PbS-MBA and PbS-MPA QDs, respectively.

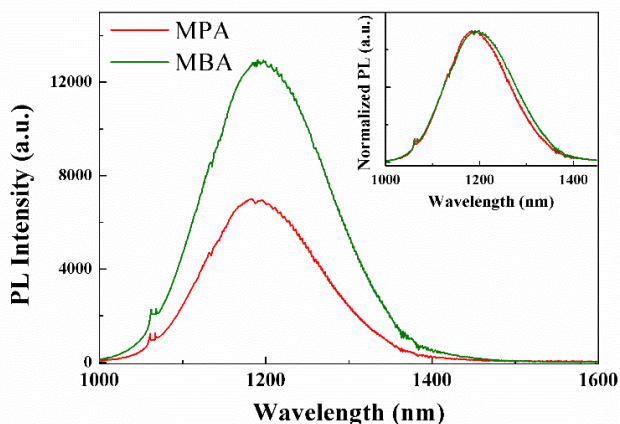


Fig. 13 Comparison of the room temperature PL spectra of PbS-MPA and PbS-MBA QD films, respectively. The inset is the normalized PL spectra.

Fig. 12 displays the  $J$ - $V$  curves and IPCE spectra of PbS QDHSCs based on MBA and MPA ligands. It was clearly shown that the  $J_{sc}$  and IPCE values in the MBA-based cell were dramatically lower than that of MPA-based cell, which indicated the very low charge collection efficiency in MBA-based cell. To investigate the charge dynamic mechanism behind the photovoltaic behaviour of MBA-based PbS QDHSCs, PL and TA spectra were measured for PbS-MBA QD films. As shown in Fig. 13, the PL peak position was identical for both MPA and MBA ligands, while PbS-MBA QDs show stronger PL intensity. This means the electronic coupling was similar for PbS-MPA and PbS-MBA QD films, and PbS-MBA QDs have less non-radiative recombination (supported by the  $V_{oc}$  decay curves in Fig. S10). Fig. 14a shows the comparison of TA spectra for PbS-MPA and PbS-MBA QD films. It can be seen that the TA curves were identical, indicating the nearly same charge transfer rate in both films. These results are conflicting with the photovoltaic properties that PbS-MBA QDs possess high charge transfer and low trap states but leads to very poor photovoltaic performances. The possible reason could be due to the situation that photo-induced charge was transferred from QDs to MBA ligands, instead of between adjacent QDs (Fig. 14b). To further investigate the unexpected charge dynamics and photovoltaic properties of PbS-MBA QDs, the energy level diagram of PbS QD, MBA and MPA was plotted and shown in Fig. S11. The energy of PbS QD was obtained from our previous work<sup>21</sup>, while that of MBA and MPA were estimated by theoretical calculation based on density functional theory (DFT) at the b3lyp/6-311g level.<sup>35</sup> It was shown that the singlet excited state (S1) energy levels of both MBA and MPA are higher than the conduction band (CB) minimum of PbS QDs. However, the S1 level of MBA is obviously lower than that of MPA, indicating their triplet excited states (T1) possess a similar trend. Although the exact T1 energy level of MBA was not obtained, it is very likely closer to the CB level of PbS QDs in comparison to that of MPA. In addition, compared with MPA, the conjugated MBA structure tends to form dimer, trimer and tetramer due to the  $\pi$ - $\pi$  stacking effect. This effect was expected to alter the T1 energy level of

stacked MBA ligands on QD surfaces, leading to the energy resonance between QDs and MBA ligands.

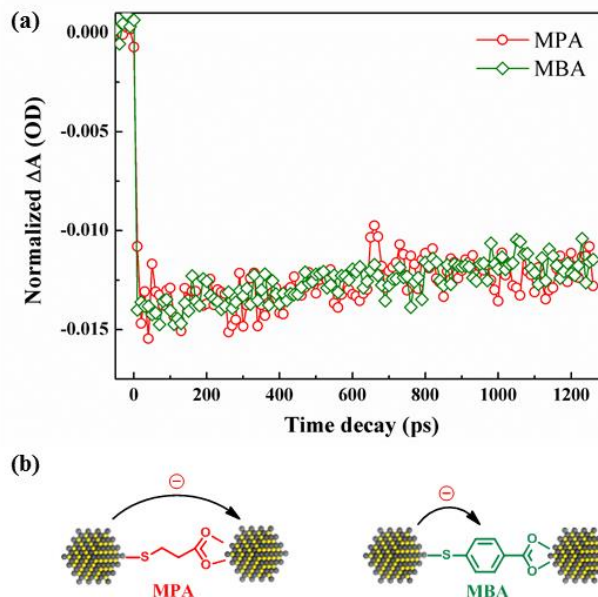


Fig. 14 (a) Comparison of the TA spectra of PbS QD films with MPA and MBA ligands, respectively. (b) Schematic view of the charge transfer process in PbS-MPA and PbS-MBA QD films.

## Conclusions

In summary, effect of ligand structure on the photovoltaic properties and charge transfer/recombination dynamics of PbS QDHSCs were systematically investigated in this study. Our findings indicate that shorter surface ligands can enhance the QD-QD coupling and thus favour the charge transfer rate in QD ensemble. On the other hand, the surface passivation and trap state of QDs are independent of the ligand length. The second shortest ligand MPA provides the best surface passivation for PbS QDs and thus leading to the highest PCE of QDHSCs in this work. The QD films with conjugated ligand MBA show stronger light harvesting and less trap states than MPA-capped QDs, but result in poor photovoltaic performances. This could be attributed to the ineffective charge transfer between adjacent QDs in the case of MBA ligands. The observed QD coupling and charge transfer process could be originated from the QD/ligand mixing and/or charge transfer from QD to MBA ligands. The obtained conclusions in this work would contribute to a deeper understanding of the exciton dynamics in QDHSCs and shed light on the further development in surface passivation and QD-based photoelectric devices.

## Acknowledgements

This research was supported by the Japan Science and Technology Agency (JST) CREST program, the PRESTO program and the MEXT KAKENHI Grant (Grant Number 26286013). Dr Chang would like to thank the Natural Science Foundation of the Higher Education Institutions of Jiangsu Province, China (16KJB430016).

## Notes and references

<sup>a</sup> Key Laboratory of Flexible Electronics (KLOFE) & Institute of Advanced Materials (IAM), Jiangsu National Synergetic Innovation Centre for Advanced Materials (SICAM), Nanjing Tech University, 30 South Puzhu Road, Nanjing 211816, China

<sup>b</sup> Faculty of Informatics and Engineering, The University of Electro-Communications, 1-5-1 Chofugaoka, Chofu, Tokyo 182-8585, Japan. Email: shen@pc.uec.ac.jp. Tel: +81 42 443 5471. Fax: +81 42 443 5501.

<sup>c</sup> Faculty of Life Science and Systems Engineering, Kyushu Institute of Technology, 2-4 Hibikino, Wakamatsu-ku, Kitakyushu, Fukuoka 808-0196, Japan.

<sup>d</sup> Department of Applied Chemistry, Chuo University, Tokyo, 112-8551, Japan.

<sup>e</sup> CREST, Japan Science and Technology Agency (JST), 4-1-8 Honcho, Kawaguchi, Saitama 332-0012, Japan.

Electronic Supplementary Information (ESI) available: [details of any supplementary information available should be included here]. See DOI: 10.1039/b000000x/

- 1 A. D. Yoffe, *Adv. Phys.*, 2002, **51**, 799-890.
- 2 A. J. Nozik, *Physica E*, 2002, **14**, 115-120.
- 3 R. D. Schaller and V. I. Klimov, *Phys. Rev. Lett.*, 2004, **92**, 186601.
- 4 G.-H. Kim, F. P. Garcia de Arquer, Y. J. Yoon, X. Lan, M. Liu, O. Voznyy, Z. Yang, F. Fan, A. H. Ip, P. Kanjanaboos, S. Hoogland, J. Y. Kim and E. H. Sargent, *Nano Lett.*, 2015, **15**, 7691-7696.
- 5 J. Du, Z. Du, J.-S. Hu, Z. Pan, Q. Shen, J. Sun, D. Long, H. Dong, L. Sun, X. Zhong and L.-J. Wan, *J. Am. Chem. Soc.*, 2016, **138**, 4201-4209.
- 6 M. J. Speirs, D. M. Balazs, H. H. Fang, L. H. Lai, L. Protesescu, M. V. Kovalenko and M. A. Loi, *J. Mater. Chem. A*, 2015, **3**, 1450-1457.
- 7 J. Tang, K. W. Kemp, S. Hoogland, K. S. Jeong, H. Liu, L. Levina, M. Furukawa, X. Wang, R. Debnath, D. Cha, K. W. Chou, A. Fischer, A. Amassian, J. B. Asbury and E. H. Sargent, *Nat. Mater.*, 2011, **10**, 765-771.
- 8 A. H. Ip, S. M. Thon, S. Hoogland, O. Voznyy, D. Zhitomirsky, R. Debnath, L. Levina, L. R. Rollny, G. H. Carey, A. Fischer, K. W. Kemp, I. J. Kramer, Z. Ning, A. J. Labelle, K. W. Chou, A. Amassian and E. H. Sargent, *Nat. Nanotech.*, 2012, **7**, 577-582.
- 9 J. M. Luther, J. Gao, M. T. Lloyd, O. E. Semonin, M. C. Beard and A. J. Nozik, *Adv. Mater.*, 2010, **22**, 3704-3707.
- 10 J. J. Choi, J. Luria, B.-R. Hyun, A. C. Bartnik, L. Sun, Y.-F. Lim, J. A. Marohn, F. W. Wise and T. Hanrath, *Nano Letters*, 2010, **10**, 1805-1811.
- 11 Z. Lingley, S. Lu and A. Madhukar, *Nano Lett.*, 2011, **11**, 2887-2891.
- 12 Z. Lingley, S. Lu and A. Madhukar, *J. Appl. Phys.*, 2014, **115**, 084302.
- 13 Y. Liu, M. Gibbs, J. Puthussery, S. Gaik, R. Ihly, H. W. Hillhouse and M. Law, *Nano Lett.*, 2010, **10**, 1960-1969.
- 14 J. Zhang, J. Tolentino, E. R. Smith, J. Zhang, M. C. Beard, A. J. Nozik, M. Law and J. C. Johnson, *J. Phys. Chem. C*, 2014, **118**, 16228-16235.
- 15 D. Tsokkou, P. Papagiorgis, L. Protesescu, M. V. Kovalenko, S. A. Choulis, C. Christofides, G. Itskos and A. Othonos, *Adv. Energy Mater.*, 2014, **4**, 1301547.
- 16 Y. Yang, W. Rodríguez-Córdoba, X. Xiang and T. Lian, *Nano Lett.*, 2011, **12**, 303-309.
- 17 A. A. Bakulin, S. Neutzner, H. J. Bakker, L. Ottaviani, D. Barakel and Z. Chen, *ACS Nano*, 2013, **7**, 8771-8779.
- 18 F. C. M. Spoor, L. T. Kunneman, W. H. Evers, N. Renaud, F. C. Grozema, A. J. Houtepen and L. D. A. Siebbeles, *ACS Nano*, 2015, **10**, 695-703.
- 19 M. Scheele, D. Hanifi, D. Zherebetsky, S. T. Chourou, S. Axnanda, B. J. Rancatore, K. Thorkelsson, T. Xu, Z. Liu, L.-W. Wang, Y. Liu and A. P. Alivisatos, *ACS Nano*, 2014, **8**, 2532-2540.
- 20 C. Giansante, I. Infante, E. Fabiano, R. Grisorio, G. P. Suranna and G. Gigli, *J. Am. Chem. Soc.*, 2015, **137**, 1875-1886.
- 21 J. Chang, Y. Kuga, I. Mora-Sero, T. Toyoda, Y. Ogomi, S. Hayase, J. Bisquert and Q. Shen, *Nanoscale*, 2015, **7**, 5446-5456.
- 22 Y. Ogomi, A. Morita, S. Tsukamoto, T. Saito, Q. Shen, T. Toyoda, K. Yoshino, S. S. Pandey, T. Ma and S. Hayase, *J. Phys. Chem. C*, 2014, **118**, 16651-16659.
- 23 N. Yuusuke, K. Takashi, O. Daisuke, H. Yoshitaka and H. Shuzi, *J. J. Appl. Phys.*, 2008, **47**, 505.
- 24 J. Chang, R. Ahmed, H. Wang, H. Liu, R. Li, P. Wang and E. R. Waclawik, *J. Phys. Chem. C*, 2013, **117**, 13836-13844.
- 25 L. C. Cass, M. Malicki and E. A. Weiss, *Anal. Chem.*, 2013, **85**, 6974-6979.
- 26 E. Lewis, S. Haigh and P. O'Brien, *J. Mater. Chem. A*, 2014, **2**, 570-580.
- 27 L. Turyanska, A. Patané, M. Henini, B. Hennequin and N. R. Thomas, *Appl. Phys. Lett.*, 2007, **90**, 101913.
- 28 J. Gao and J. C. Johnson, *ACS Nano*, 2012, **6**, 3292-3303.
- 29 Q. Shen, Y. Ogomi, B.-w. Park, T. Inoue, S. S. Pandey, A. Miyamoto, S. Fujita, K. Katayama, T. Toyoda and S. Hayase, *Phys. Chem. Chem. Phys.*, 2012, **14**, 4605-4613.
- 30 M. Ono, T. Nishihara, T. Ihara, M. Kikuchi, A. Tanaka, M. Suzuki and Y. Kanemitsu, *Chem. Sci.*, 2014, **5**, 2696-2701.
- 31 R. A. Marcus and N. Sutin, *Biochimica et Biophysica Acta*, 1985, **811**, 265-322.
- 32 R. R. Haering and E. N. Adams, *Phys. Rev.*, 1960, **117**, 451-454.
- 33 R. Schmechel and H. von Seggern, *Phys. Stat. Sol. (a)*, 2004, **201**, 1215-1235.
- 34 A. Baumann, S. Văth, P. Rieder, M. C. Heiber, K. Tvingstedt and V. Dyakonov, *J. Phys. Chem. Lett.*, 2015, **6**, 2350-2354.
- 35 D. B. Axel, *J. Chem. Phys.*, 1993, **98**, 5648-5652.